

Dual-Active-Bridge converter cascaded regulators gains selection by means of the D-decomposition technique

Abstract. Neimark's D-decomposition technique as a power-full graphical tool to select DAB compensators gains was presented. Technique for inner current and outer voltage regulators was used. Gains based on identified boost transfer functions were selected. Time responses from calculations were calculated and experimentally verified at the laboratory setup.

Streszczenie. Została przedstawiona technika D-rozbicia Neimarka, jako graficzne narzędzie do wyboru wzmacniń przekształtnika z podwójnym mostkiem aktywnym. Wykorzystano technikę dla regulatora prądu wyjściowego i napięcia wyjściowego. Wzmacnienia wyznaczono na podstawie eksperymentalnie zidentyfikowanych transmittancji. Odpowiedzi czasowe zostały zweryfikowane eksperymentalnie w laboratorium. (Dobór nastaw przekształtnika z podwójnym mostkiem aktywnym w kaskadowej strukturze regulacji za pomocą techniki D-rozbicia)

Keywords: D-decomposition technique, global stability boundary, frequency and time domain constraints, DAB converter, cascaded control

Słowa kluczowe: technika D-rozbicia, granica stabilności, ograniczenia w dziedzinie częstotliwości i czasu, przekształtnik z podwójnym mostkiem aktywnym, kaskadowa struktura regulacji

Introduction

Nowadays, the control of power electronics devices is still challenging. That is truth because a lot of control techniques exists, [1, 2]. There is no one right way to have good performance in every case. Well-known solutions are used to select the structure and tune the gains [1, 3]. This group includes basic criteria such as: Nyquist, pole placement, etc. In the field of converters regulation, numerous control techniques, including the widely employed Proportional Integral Derivative (PID) controller, are available [4]. The PID control is a well-established and widely used control technique that is relatively simple to implement and can achieve good results in many cases, as proven by its use in over 90% of industrial applications. To achieve stable and fast control, several approaches for determining PID controller gains have been developed for tuning [1, 5]. Another good dynamic performance ensure are technique based on the neural networks [6] or genetic algorithms [7]. In recent years, \mathfrak{D} -decomposition, also called \mathfrak{D} -partitioning, has emerged as a technique for converters controller design. This method aims to simplify the control problem. The application of \mathfrak{D} -decomposition in cascaded controller design for Dual Active Bridge converters (DAB) represents a significant step in achieving high-performance control under dynamic conditions. The flexibility and features offered by the cascaded architecture, combined with the adaptability of \mathfrak{D} -decomposition, make it a compelling choice for modern power electronics applications.

The paper [8] discusses the selection of tuning parameters for SVCs used for voltage stabilization in power systems. It compares traditional methods based on solving differential equations with the \mathfrak{D} -decomposition method, which can determine stable tuning parameters without solving the system of differential equations. The results show that the \mathfrak{D} -decomposition method is a valid approach for choosing SVC tuning parameters when the value of the controller gain or time constant is given. Article [9] proposes a visual analysis method based on the \mathfrak{D} -decomposition to present the performance of cascaded control system for Power Conversion Systems (PCS) with optional parameters of mobile energy storage system. The dual loop model of PCS is established, and stability regions based on regulator parameters are obtained via the \mathfrak{D} -decomposition technique. The influence of regulator parameters, load variation, and electrical parameters selection on loop performance is analyzed, and the theoretical analysis is verified on a laboratory PCS platform. Authors in paper [10] propose a hierarchical mode-

dispatching control strategy for multi-inverter power stations, which solves the small-signal stability or oscillation problem caused by changes in the structure and parameters of the system and the grid. The top control layer based mode-dispatching control (\mathfrak{D} -decomposition technique), while the bottom control layer adopts impedance adaptive dual-mode control for each inverter. The proposed strategy achieves fast dynamic cooperation of multi-inverter power stations and ensures effective oscillation suppression under the rapid changes of grid characteristics and inverter plug-and-play. In summary, Neimark's \mathfrak{D} -decomposition method is a graph-theoretic method used to select controllers gains.

In this article the basic DAB converter as simple and effective way to control output voltage is analysed. DAB converter is used in lot of areas, because of their advantage and are commonly used in industrial electronics for a variety of applications. DAB converters are used to provide a stable output voltage for a wide range of electronic devices. They are commonly used in power supplies for electronic equipment [3, 11, 12]. DAB converters are used in electric vehicles [13] to step up the voltage from the battery to power the motor. This allows for greater efficiency and longer range. Presented topology is used in renewable energy systems [14], such as solar [4] and wind power [15], to adjust the voltage output of the energy source to a voltage that can be used to supply homes and businesses. DAB converters are used in battery charging systems [16] to increase the voltage of the charging current. This allows for faster charging times and more efficient use of the charging energy. The DAB converter can operate in both power transfer directions, allowing energy to flow in either direction between the input and output. This makes bidirectional DAB converters useful in applications where voltage needs to be stepped up or down. The integration of DAB converters into microgrids and hybrid energy systems requires coordinated control strategies to ensure smooth power transfer and seamless transition between grid-connected and islanded modes. Advanced control schemes, such as droop control and virtual impedance control, have been proposed to enable stable grid integration and enhanced power sharing among distributed energy resources.

This paper is organized as following. The first section contains the analysed system details. Next section, the \mathfrak{D} -decomposition technique is presented to select inner and outer controller gains. The presented methodology includes formulas for PI type controllers. Next, identification of the

converter transfer functions is presented. Then controller design methodology for reference frequency and for cascaded structure is presented. Experimental results with the PI regulators are presented and discussed. Finally conclusions are given.

The Dual Active Bridge converter as a object under control

The Dual Active Bridge converter electrical circuit used in this article for identification, current, voltage and cascaded control can be seen in Fig. 1.

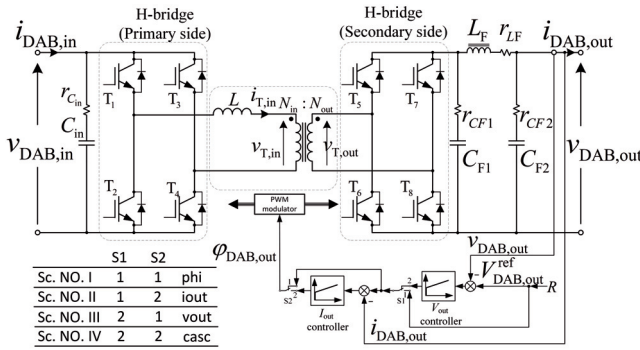


Fig. 1. Cascaded control DAB general circuit. Control configurations: scenario No. I) - for the identification; scenario No. II) - for the output current control; scenario No. III) - for the voltage control; scenario No. IV) - for the cascaded control

Cascaded control general circuit (Fig. 1) has been directly implemented in the laboratory setup. The rated DC output voltage ($V_{DAB,out}$) was chosen to be equal to 50 V, and this with input rated voltage ($V_{DAB,in}$) set to 100 V. Rated output power ($P_{DAB,out}$) was assumed as 225 W. The F450R12KS4 IGBT modules were used as the switching devices. As the signal processing and control platform the Texas Instruments TMS320F28379D board with 32 kHz control loop frequency was used. The PWM switching frequency was set to constant value of 16 kHz.

As the DAB power transfer control method the Single Phase Shift modulation (SPS) was used. The method is basing on variation of the phase shift ($\varphi_{DAB,out}$) between the input voltage side and the output voltage side gate drive signals. The duty cycle of all the gate drive signals is set to 50 %. The dead time of 1 μ s is applied between the upper and the lower signals in order to avoid the short circuits in between switching. In case of low on-state resistance MOS-FET switches are used the general circuit may need to be changed. By changing the phase shift, the power transfer is controlled basing on variation of the L inductance current which is the same as the input transformer current.

Developed test circuit was verified through measurement of its output power within assumed output voltage tolerance $V_{DAB,out}^{tol} = \pm 10\%$ in function of the φ_{out} . The results can be seen in Fig. 2.

$$(1) \quad G_{CL}^{r2\#}(s) = \frac{G_{DAB}^{c2\#}(s)G_{PWM}(s)(k_3C^v(s) + k_4C^i(s)(k_2 + k_1C^v(s)))}{1 + G_{A2D}^i(s)G_{DAB}^{c2i_{out}}(s)G_{PWM}(s)k_4C^i(s) + G_{A2D}^v(s)G_{DAB}^{c2v_{out}}(s)G_{PWM}(s)(k_3 + k_1k_4C^i(s))C^v(s)}$$

where: $\# \rightarrow v_{out}$ if reference-to-output voltage or $\# \rightarrow i_{out}$ if reference-to-output current

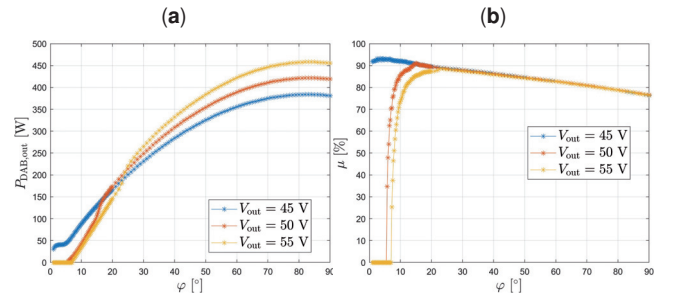


Fig. 2. Experimentally measured DAB output power ($P_{DAB,out}$) (a) and efficiency (μ) (b) at minimum (v_{min}) and maximum (v_{max}) output voltage ($V_{DAB,out} \in \{45, 50, 55\}$ V). Plots measured for $L = 140 \mu$ H, and $V_{in} = 100$ V. Output power shows the impact of the dead time [17]

\mathfrak{D} -decomposition technique for cascaded control structure

The \mathfrak{D} -decomposition technique was proposed by Neimark in 1948 [18]. Generally speaking, it establishes direct correlation between the characteristics equation and the space of permissible parameters for which the global stability is met. Principles of this technique, gain selection for ideal and with time delays control structure are presented in [19]. Additionally, the gain and phase margin for the first order plant were presented in [5].

The \mathfrak{D} -decomposition technique is gaining popularity as a method for controller design [10, 20, 21]. It offers a systematic approach for selecting inner and outer controller gains, which can lead to improved control performance.

For controllers design control structure with voltage and current transfer function as shown in Fig. 3 will be used. The closed-loop transfer function of the selected control structure can be written as shown in Eq. 1. Equation consist of the characteristic equation used in this article together with \mathfrak{D} -decomposition technique to calculate controllers gains.

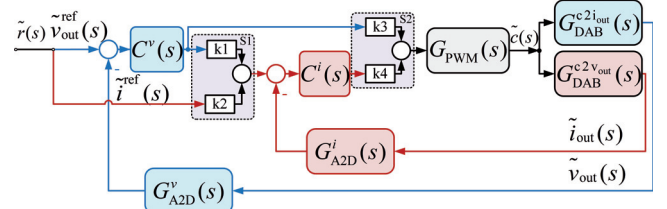


Fig. 3. Block diagram of the cascaded closed-loop control structure with the PWM and the A2D delays represented by the $G_{PWM}(s) = e^{-s\tau_{PWM}}$ and $G_{A2D}(s) = e^{-s\tau_{A2D}}$ transfer function respectively. DAB transfer functions are represented by the current, $G_{DAB}^{c2i_{out}}$, and voltage, $G_{DAB}^{c2v_{out}}$, transfer function.

At first, to introduce frequency domain constraints, denominator of the closed-loop transfer function (1) can be written by replacing the point $(-1, j0)$ with a certain location on the complex surface: $(a + jb) + G_{OL}^{r2\#}(s)$, where $(a + jb)$ denotes the desired location of any arbitrary point in Cartesian coordinates. Using the notation $\#$ it is possible to write the general form for voltage ($\# \rightarrow v_{out}$) or current controller ($\# \rightarrow i_{out}$). Next, to introduce "s" domain constraints, operator Laplace can be extended as $s = \sigma + j\omega_d$. Elements $A_n^{r2\#}(s)$ takes the form $A_n^{r2\#}(\sigma + j\omega_d)$ and can be

represented as real ($\Re[A_n^\#(\sigma + j\omega_d)]$) and imaginary part ($\Im[A_n^{r2\#}(\sigma + j\omega_d)]$). These steps give an opportunity to determine K_P and K_I gains for frequency and "s" domain.

$$(2) \quad K_P^{r2\#} = C_1 / ((\Re[A_2^{r2\#}(\sigma + j\omega_d)]^2 + \Im[A_2^{r2\#}(\sigma + j\omega_d)]^2) \omega_d)$$

$$(3) \quad K_I^{r2\#} = C_2 / ((\Re[A_2^{r2\#}(\sigma + j\omega_d)]^2 + \Im[A_2^{r2\#}(\sigma + j\omega_d)]^2) \omega_d)$$

where C_1 and C_2 were explained at the bottom of the page.

Formulas (2) and (3) can be used for current, voltage or cascaded control structure (Fig. 3). Parts $A_n^{r2\#}(s)$ of the Eq. 2 and Eq. 3 were presented below.

$$(4) \quad A_1^{r2v_{out}}(s) = G_{A2D}^i(s) G_{DAB}^{c2i_{out}}(s) G_{PWM}(s) k_4 C^i(s)$$

$$(5) \quad A_2^{r2v_{out}}(s) = G_{A2D}^v(s) G_{DAB}^{c2v_{out}}(s) G_{PWM}(s) (k_3 + k_1 k_4 C^i(s))$$

$$(6) \quad A_1^{r2i_{out}}(s) = G_{A2D}^v(s) G_{DAB}^{c2v_{out}}(s) G_{PWM}(s) k_3 C^v(s)$$

$$(7) \quad A_2^{r2i_{out}}(s) = G_{A2D}^i(s) G_{DAB}^{c2i_{out}}(s) G_{PWM}(s) k_4 + G_{A2D}^v(s) G_{DAB}^{c2v_{out}}(s) G_{PWM}(s) k_1 k_4 C^v(s)$$

Identification of the control-to-output Dual Active Bridge converter transfer functions

Control-to-output voltage ($c2v_{out}$) and control-to-output current ($c2i_{out}$) transfer functions using frequency response analysis were obtained. To estimate transfer functions frequency response analysis with 200 points and sine wave were used. Results in form of the Bode plot for the operating point $P_{DAB,out}^{rtd} = 225$ W can be seen in Fig. 4 and Fig. 5 respectively, for voltage and current transfer functions.

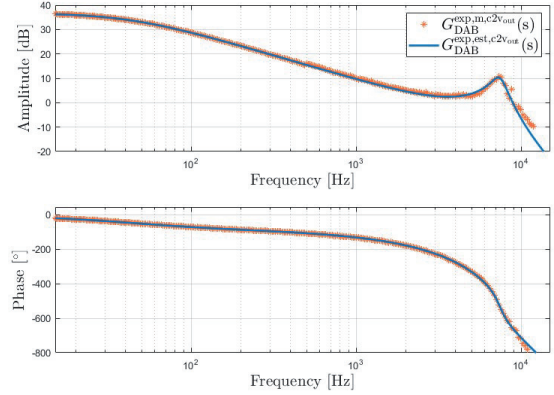


Fig. 4. The Bode plot of the identified DAB control-to-output voltage transfer function measured for the operating point $P_{DAB,out}^{rtd} = 225$ W with coefficient FIT = 99.02%

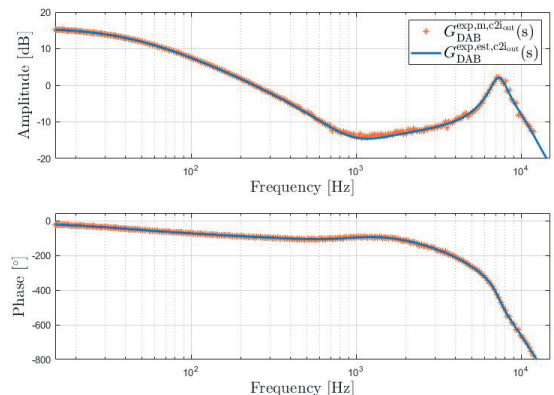


Fig. 5. The Bode plot of the identified DAB control-to-output current transfer function measured for the operating point $P_{DAB,out}^{rtd} = 225$ W with coefficient FIT = 98.29%

This two transfer functions using Matlab `ttest` function were estimated with *FIT* at the level of 98-99 %, where *FIT* coefficient as 100(1-(Normal Root Mean Square Error, NRSME)) were calculated. Additionally, numbers of the coefficient numerator and denominator polynomials based on experimentally measured point coverage over a wide frequency range were selected. Results in mathematical formulas in Eq. 8 and Eq. 9 were given.

Controller design criterion

In this section, using the \mathfrak{D} -decomposition technique, the DAB output voltage time response results, which incor-

$$C_1 = \left(-a \Im[A_2^\#(\sigma + j\omega_d)] + \Im[A_2^\#(\sigma + j\omega_d)] \Re[A_1^\#(\sigma + j\omega_d)] + (b - \Im[A_1^\#(\sigma + j\omega_d)]) \Re[A_2^\#(\sigma + j\omega_d)] \right) \sigma + \left(b \Im[A_2^\#(\sigma + j\omega_d)] + \Im[A_1^\#(\sigma + j\omega_d)] \Im[A_2^\#(\sigma + j\omega_d)] + (a - \Re[A_1^\#(\sigma + j\omega_d)]) \Re[A_2^\#(\sigma + j\omega_d)] \right) \omega_d$$

$$C_2 = (\sigma^2 + \omega_d^2) \left(a \Im[A_2^\#(\sigma + j\omega_d)] - \Im[A_2^\#(\sigma + j\omega_d)] \Re[A_1^\#(\sigma + j\omega_d)] + \Re[A_2^\#(\sigma + j\omega_d)] (-b + \Im[A_1^\#(\sigma + j\omega_d)]) \right)$$

$$(8) \quad G_{DAB}^{\text{exp,est},c2v_{out}}(s) = \frac{-4.56 \cdot 10^2 s^2 - 2.25 \cdot 10^7 s - 6.40 \cdot 10^{11}}{s^3 + 9.01 \cdot 10^3 s^2 + 1.98 \cdot 10^7 s + 5.32 \cdot 10^{11}}$$

$$(9) \quad G_{DAB}^{\text{exp,est},c2i_{out}}(s) = \frac{1.99 \cdot 10^2 s^4 + -1.08 \cdot 10^7 s^3 + 3.07 \cdot 10^{11} s^2 + 1.71 \cdot 10^{15} s + 1.43 \cdot 10^{19}}{s^5 + 4.97 \cdot 10^4 s^4 + 2.77 \cdot 10^9 s^3 + 9.12 \cdot 10^{13} s^2 + 5.28 \cdot 10^{17} s + 1.34 \cdot 10^{20}}$$

porates reference value of the frequencies of the oscillation, was presented. For this purpose, one fixed frequency ($f^{\text{ref}} = 200$ Hz) and four different values of phase margin ($PM \in \{15, 30, 45, 60\}$) was selected for output voltage closed-loop control structure (scenario No.III from Fig.3). Output voltage step response from 45 to 50 V for mathematical model and experimental setup in Fig. 6 were presented.

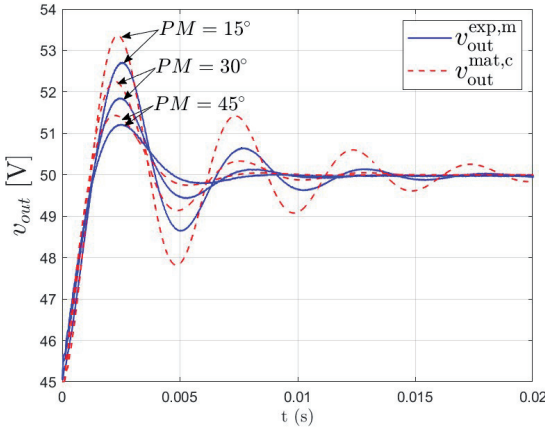


Fig. 6. Mathematically calculated, $v_{\text{out}}^{\text{mat},c}$, and experimentally measured, $v_{\text{out}}^{\text{exp},m}$ step responses for the reference phase margin $PM \in \{15, 30, 45\}^\circ$ and reference frequency $f^{\text{ref}} = 200$ Hz

Measured frequencies for mathematical and experimental results from Fig. 6 does not correspond to value of reference frequency for any $PM \in \{15, 30, 45\}^\circ$. They are 197, 171, 146 and 201, 189, 161 Hz respectively for experimentally measured and mathematically calculated output voltage ($v_{\text{out}}^{\text{exp},m}$ and $v_{\text{out}}^{\text{mat},c}$). For this reason, the reference phase margin was changed to a damping ratio and the voltage controller gains were recalculated. Results for the reference damping ratio $\xi \in \{0.3, 0.4, 0.6, 0.7\}$ in Fig. 7 were presented.

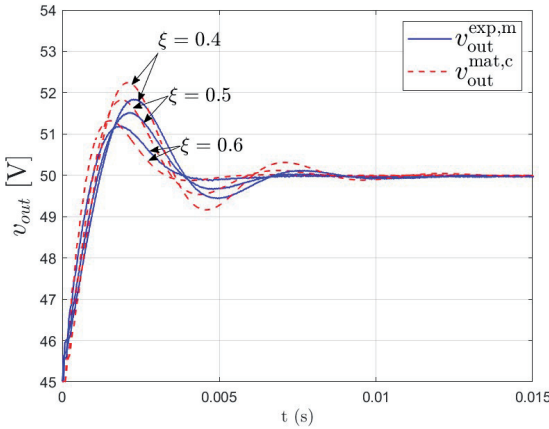


Fig. 7. Mathematically calculated, $v_{\text{out}}^{\text{mat},c}$, and experimentally measured, $v_{\text{out}}^{\text{exp},m}$ step responses for the reference damping ratio $\xi \in \{0.3, 0.4, 0.6, 0.7\}$ and reference frequency $f^{\text{ref}} = 200$ Hz

In case of the damping ratio is used with \mathfrak{D} -decomposition, measured frequency of the step response oscillation are the same as reference frequency. This approach in next section was used to calculate inner and outer controller gains.

Cascaded Controller design

At first, the \mathfrak{D} -decomposition technique for the DAB inner current controller was used. Results in the form of hyper-surfaces are more complicated, than in case of simple ob-

ject model. In other words, selection of controllers areas requires some simplification, by applying frequency limits, to find non zero regions. This approach is required when larger constraints values are used, but this approach should not be used with global stability boundary. Using \mathfrak{D} -decomposition, the frequency domain constraints to indicate K_p - K_i plane were introduced.

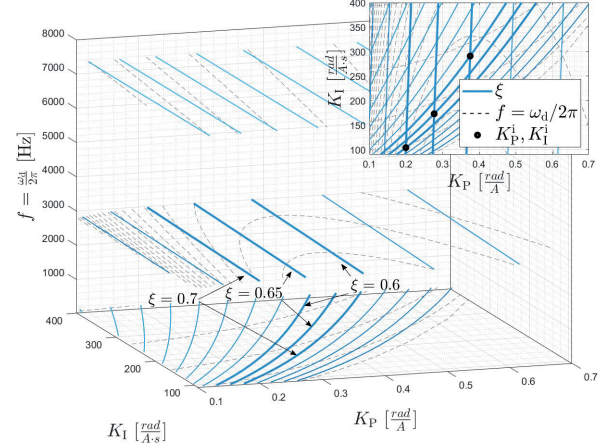


Fig. 8. Visualisation of the current regulator 3D boundaries and zoom in 2D with upper frequency limit $f^{\text{max}} = 4$ kHz. Results were obtained for damping ratio ξ (blue line) and damped natural frequency ω_d (dotted line)

Fig. 8 presents complex controller gains map with particular insight in object dynamics and was used in further research. In this article points for current controller were selected for three values of the damping ratio ($\xi \in \{0.6, 0.65, 0.7\}$) and upper frequency limit $f^{\text{max}} = 4$ kHz. The current controller gains were selected for maximum frequency understood as $\omega_d/2\pi$ and are $K_p^i \in \{0.376, 0.277, 0.199\}^{\text{rad}/A}$, $K_i^i \in \{291.0, 173.2, 104.1\}^{\text{rad}/A \cdot s}$. Basing on these values together with \mathfrak{D} -decomposition technique and damping ratio $\xi = 0.9$ outer voltage PI regulator $K_p^v \in \{0.257, 0.406, 0.631\}^A/v$ and $K_i^v \in \{135.2, 314.6, 568.7\}^A/v \cdot s$ gains were selected. Visualisation of the voltage controller gains for current gains for $\xi = 0.7$ in (Fig. 9) were presented. Voltage controller gains for the same frequency range and value the damping ratio $\xi = 0.9$ were obtained.

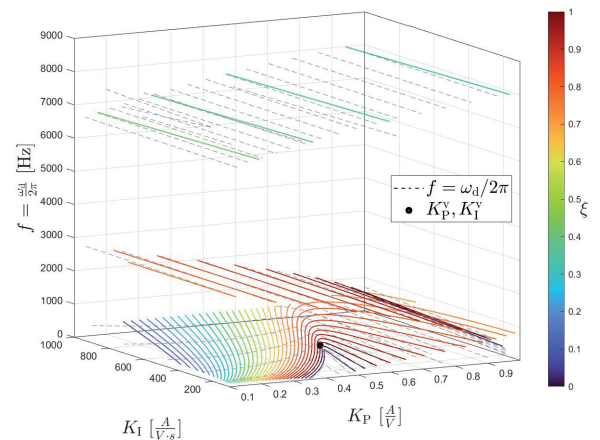


Fig. 9. Determination of the voltage PI controller for one point $K_p^i = 0.199 \text{ rad}/A$ and $K_i^i = 104.1 \text{ rad}/A \cdot s$ from Fig. 8. Selected $K_p^v = 0.631 A/v$ and $K_i^v = 568.6 A/v \cdot s$ gains corresponding to $\xi = 0.9$ and $f = \frac{\omega_d}{2\pi} = 195$ Hz

Experimental results

Obtained results were confirmed at the laboratory setup (Fig. 10). The experimental tests were performed at the rated output power of the DAB converter ($P_{\text{DAB,out}}^{\text{rtd}} = 225 \text{ W}$) with 10 % voltage step around the rated output voltage $V_{\text{DAB,out}}^{\text{rtd}} = 50 \text{ V}$ (Fig. 11a and 11c) and additionally output power to 250 W was changed (Fig. 11b and 11d)

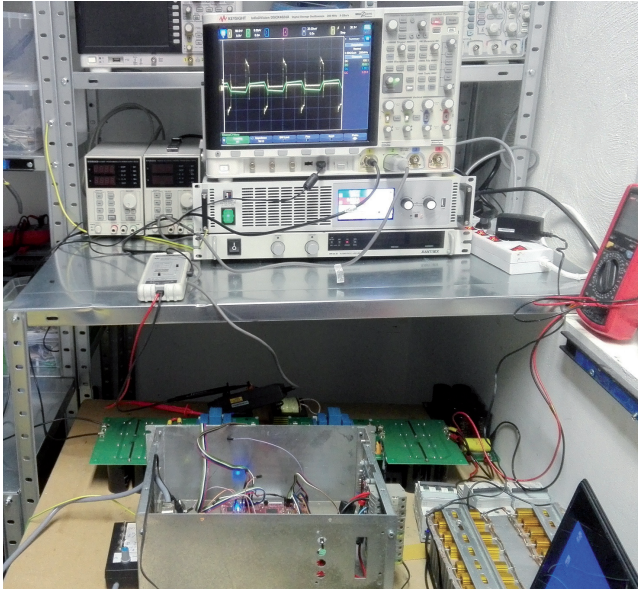


Fig. 10. Laboratory setup included power supply, DAB converter and electronic load

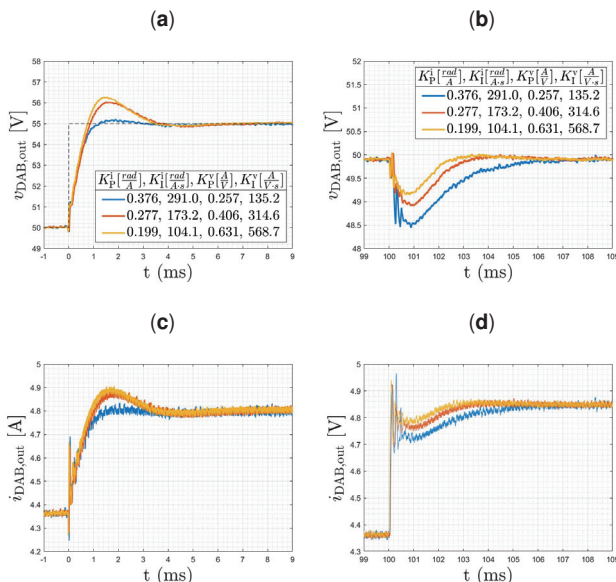


Fig. 11. DAB converter output voltages ($v_{\text{DAB,out}}$) (a, b) and output current ($i_{\text{DAB,out}}$) (c, d) step responses of output voltages ($v_{\text{DAB,out}}$) from 50 to 55 V (a, c) and output power ($P_{\text{DAB,out}}$) from 225 to 250 W (b, d). Results measured from experimental setup (Fig. 10) for three set of K_p , K_i values

Conclusion

Controller design is a critical aspect of power electronics, as it determines the efficiency, stability, and performance of power converters. Graphical interpretation of the \mathfrak{D} -decomposition results can be neglected and only mathematical formulas can be used to find controllers gains. This approach can be easily implemented in real time solution e.g. FPGA. While \mathfrak{D} -decomposition presents significant potential, challenges still exist in implementing this technique in real-

time embedded systems.

In conclusion, \mathfrak{D} -decomposition stands as a promising and innovative approach to set control DAB converters. By simplifying the control problem and enabling localized control adaptation, this technique offers enhanced performance, frequency insight, and flexibility in addressing the dynamic behaviour of DAB converters. Further research will pave the way for the effective integration of \mathfrak{D} -decomposition into practical applications, contributing to the advancement of power electronics and sustainable energy systems.

Table 1. Parameters of the DAB converter

Parameter	Value
Input voltage, $V_{\text{DAB,in}}^{\text{rtd}}$	100 VDC
Output voltage, $V_{\text{DAB,out}}^{\text{rtd}}$	50 VDC
Rated output power, $P_{\text{DAB,out}}^{\text{rtd}}$	225 W
Output voltage tolerance, $V_{\text{DAB,out}}^{\text{tol}}$	$\pm 10\%$
Inductance, L	140 μH
Input capacitance, C_{in}	373 μF
Input capacitor esr, $r_{C,\text{in}}$	80 m Ω
Output capacitance, C_{F1}	425 μF
Output capacitor esr, r_{CF1}	88 m Ω
Output capacitance, C_{F2}	16 μF
Output capacitor esr, r_{CF2}	10 m Ω
Output inductance, L_{F}	21 μH
Output inductance esr, r_{LF}	7 m Ω
Transformer ratio, n	2
PWM frequency, f_{PWM}	16 kHz
A2D frequency, f_{A2D}	32 kHz
Assumed efficiency, μ	85 %

Authors: Karol Najdek DSc, Radosław Nalepa DSc, Division of Power Networks and Systems, Department of Electrical Power Engineering, Faculty of Electrical Engineering, Wrocław University of Science and Technology, Wybrzeże Wyspiańskiego 27, 50-370 Wrocław, Poland, email: karol.najdek@pwr.edu.pl

REFERENCES

- [1] K. J. Astrom, T. Hägglund, and K. J. Astrom, *Advanced PID control*. ISA-The Instrumentation, Systems, and Automation Society Research Triangle, 2006, vol. 461.
- [2] G. F. Franklin, J. D. Powell, A. Emami-Naeini, and H. Sanjay, *Feedback control of dynamic systems*. Pearson London, 2015.
- [3] F. Blaabjerg, *Control of Power Electronic Converters and Systems: Volume 1*. Academic Press, 2018, vol. 1.
- [4] Y. Gu, W. Li, and X. He, "Passivity-based control of dc microgrid for self-disciplined stabilization," *IEEE Transactions on Power Systems*, vol. 30, no. 5, pp. 2623–2632, 2015.
- [5] K. Najdek and R. Nalepa, "The frequency- and the time-domain design of a dual active bridge converter output voltage regulator based on the d-decomposition technique," *IEEE Access*, vol. 9, pp. 71 388–71 405, 2021.
- [6] X. Meng, Y. Jia, Q. Xu, C. Ren, X. Han, and P. Wang, "A novel intelligent nonlinear controller for dual active bridge converter with constant power loads," *IEEE Transactions on Industrial Electronics*, vol. 70, no. 3, pp. 2887–2896, 2023.
- [7] T. Eberle, A. Jalilian, N. Weitz, and M. März, "Performance enhancement of a dual active bridge by a genetic algorithm based routine for optimal parameters of a cascade control," pp. 2767–2774, 2023.
- [8] E. Jaramillo-Leon and R. R. Karymov, "Application of the d-decomposition method using one parameter to select tuning parameters of static var compensators," pp. 1–6, 2022.
- [9] H. Li, Y. Tao, Z. Dai, P. Qian, C. Zhou, H. Yu, and G. Li, "Visual analysis of pcs cascaded control system based on d-partition method," in *2022 IEEE 3rd China International Youth Conference on Electrical Engineering (CIYCEE)*, 2022, pp. 1–7.
- [10] M. Li, H. Geng, and X. Zhang, "Hierarchical mode-dispatching control for multi-inverter power stations," *IEEE Transactions on*

- Industrial Electronics*, pp. 1–10, 2022.
- [11] M. F. G. B. C. Kuo, *Automatic control systems*. McGraw-Hill Education, 2017.
 - [12] F. Krismer and J. W. Kolar, “Efficiency-optimized high-current dual active bridge converter for automotive applications,” *IEEE Transactions on Industrial Electronics*, vol. 59, no. 7, pp. 2745–2760, 2012.
 - [13] S. Ghosh and B. Singh, “A reconfigurable dual active bridge converter with wide zvs range for charging of electric vehicles,” pp. 1–6, 2020.
 - [14] F. Blaabjerg, *Control of Power Electronic Converters and Systems: Volume 2*. Academic Press, 2018, vol. 2.
 - [15] M. Guan, “A series-connected offshore wind farm based on modular dual-active-bridge (dab) isolated dc–dc converter,” *IEEE Transactions on Energy Conversion*, vol. 34, no. 3, pp. 1422–1431, 2019.
 - [16] N. Naik, C. Vyjayanthi, and C. Modi, “Filter-based active damping of dab converter to lower battery degradation in ev fast charging application,” *IEEE Access*, vol. 11, pp. 74 277–74 289, 2023.
 - [17] R. Barlik, M. Nowak, and P. Grzejszczak, “Power transfer analysis in a single phase dual active bridge,” *Bulletin of the Polish Academy of Sciences. Technical Sciences*, vol. 61, no. 4, 2013.
 - [18] Y. I. Neimark, “Ob opriedieniji znaczenij parametrow, pri kotorych sistemi awtomatyczeskogo riegliriowanja ustojcziwa,” *Awtomatika i Telemiechanika*, vol. 3, 1948.
 - [19] Z. Shafiei and A. Shenton, “Relative stability for open-loop stable and unstable discrete control systems with perturbed or adjustable parameters,” pp. 2180–2185, 1999.
 - [20] M. Li, X. Zhang, Z. Guo, H. Pan, M. Ma, and W. Zhao, “Impedance adaptive dual-mode control of grid-connected inverters with large fluctuation of scr and its stability analysis based on d-partition method,” *IEEE Transactions on Power Electronics*, vol. 36, no. 12, pp. 14 420–14 435, 2021.
 - [21] K. Najdek and R. Nalepa, “Dobór nastaw regulatora napięcia konwertera z podwójnym mostkiem aktywnym za pomocą techniki d-rozbicia rozszerzonej o funkcję mapującą ułatwiającą unikanie nasycania,” *XV Konferencja Naukowa Sterowanie w Energoelektronice i Napędzie Elektrycznym SENE 2022*, 2022.